NMR Structures of the C-Terminal Segment of Surfactant Protein B in Detergent Micelles and Hexafluoro-2-propanol†

Valerie Booth,*,‡ Alan J. Waring,§,|| Frans J. Walther,§ and Kevin M. W. Keough‡

Department of Biochemistry, Memorial University of Newfoundland, St. John's, Newfoundland A1B 3X9, Canada, LA Bio Med at Harbor-University of California Los Angeles Medical Center, Torrance, California 90502, and Department of Medicine, University of California Los Angeles School of Medicine, Los Angeles, California 90095

Received August 20, 2004; Revised Manuscript Received September 22, 2004

ABSTRACT: Although the membrane-associated surfactant protein B (SP-B) is an essential component of lung surfactant, which is itself essential for life, the molecular basis for its activity is not understood. SP-B's biophysical functions can be partially mimicked by subfragments of the protein, including the C-terminus. We have used NMR to determine the structure of a C-terminal fragment of human SP-B that includes residues 63−78. Structure determination was performed both in the fluorinated alcohol hexafluoro-2-propanol (HFIP) and in sodium dodecyl sulfate (SDS) micelles. In both solvents, residues 68−78 take on an amphipathic helical structure, in agreement with predictions made by comparison to homologous saposin family proteins. In HFIP, the five N-terminal residues of the peptide are largely unstructured, while in SDS micelles, these residues take on a well-defined compact conformation. Differences in helical residue side chain positioning between the two solvents were also found, with better agreement between the structures for the hydrophobic face than the hydrophilic face. A paramagnetic probe was used to investigate the position of the peptide within the SDS micelles and indicated that the peptide is located at the water interface with the hydrophobic face of the helix oriented inward, the hydrophilic face of the helix oriented outward, and the N-terminal residues even farther from the micelle center than those on the hydrophilic face of the α-helix. Interactions of basic residues of SP-B with anionic lipid headgroups are known to have an impact on function, and these studies demonstrate structural ramifications of such interactions via the differences observed between the peptide structures determined in HFIP and SDS.

Lung surfactant is essential for normal breathing due to its ability to reduce alveolar surface tension to extremely low values, thus preventing alveolar collapse during expiration and reducing the work of breathing. Surfactant is synthesized and secreted into the alveolar fluid by type II pneumocytes and is composed of approximately 80% phospholipids, 10% neutral lipids, and 10% proteins (*1*, *2*). Surfactant-associated water soluble proteins A and D (SP-A and SP-D, respectively) are important for host defense (*3*, *4*) but have less impact than the hydrophobic surfactant proteins on the biophysical properties of bilayers and monolayers. By contrast, the presence of hydrophobic surfactant proteins B and C (SP-B[1] and SP-C, respectively) is critical for optimizing surface tension reduction (*5*).

Deficiency in lung surfactant leads to conditions such as neonatal respiratory distress syndrome (RDS), which is a crucial problem in premature newborns (*6*), as well as acute respiratory distress syndrome (ARDS) (*7*), a sudden lung failure associated with acute injury or illness. The clinical introduction of surfactant replacement therapy in the early 1990s dramatically improved pulmonary morbidity and mortality in premature infants with RDS (*8*) and may also be effective in ARDS (*9*). Clinical trials have found that artificial surfactants which include SP-B and SP-C are much more efficacious than protein-free surfactant preparations (*10*). SP-B fulfils a crucial role since hereditary SP-B deficiency is lethal in humans (*11*) and in SP-B knockout mice (*12*), while antibodies against SP-B cause RDS *in vivo* (*13*). SP-C deficiency is not lethal at birth (*14*) but is associated with familial interstitial lung disease (*15*), and its absence modifies the biophysical properties of monolayers (*14*).

Biophysical studies of SP-B have yielded a long list of *in vitro* activities that may be important in SP-B's *in vivo* roles,

† The researchers acknowledge financial support from the Canadian Institutes of Health Research, Health Canada, and the National Institutes of Health (Grant R01 HL55534). V.B. is a Parker B. Francis Fellow in Pulmonary Research.

* To whom correspondence should be addressed. E-mail: valerie@physics.mun.ca. Phone: (709) 737-4523. Fax: (709) 737-8739.

‡ Memorial University of Newfoundland.

§ LA Bio Med at Harbor-University of California Los Angeles Medical Center.

|| University of California Los Angeles School of Medicine.

[1] Abbreviations: MALDI-TOF, matrix-assisted laser desorption time-of-flight; HPLC, high-performance liquid chromatography; EDT, ethanedithiol; TFA, trifluoroacetic acid; HMP, 4-hydroxymethylphenoxyacetyl-4′-methylbenzyhydrylamine resin; HFIP, hexafluoro-2-propanol; TFE, trifluoroethanol; SDS, sodium dodecyl sulfate; DSA, 5-doxylstearic acid; DSS, 2,2-dimethyl-2-silapentane-5-sulfonic acid; NOE, nuclear Overhauser effect; NOESY, nuclear Overhauser enhancement spectroscopy; TOCSY, total correlation spectroscopy; HSQC, heteronuclear single-quantum coherence; SP-B, surfactant protein B; SP-B_{CTERM}, residues 63−78 of SP-B; DPPC, dipalmitoylphosphatidylcholine; RDS, respiratory distress syndrome; ARDS, acuate respiratory distress syndrome; FTIR, Fourier transform infrared; CSI, chemical shift index.

10.1021/bi0481895 CCC: $27.50
Published on Web 11/10/2004

including membrane binding, membrane lysis, membrane fusion, promotion of lipid adsorption to air−liquid surfaces, stabilization of monomolecular surface films, and respreading of films from collapsed phases (reviewed in ref *5*). SP-B preferentially associates with anionic lipids in surface monolayers (*16*), and upon compression of the film, the SP-B−anionic lipid network forms buckled structures that remain attached to the monolayer (*17*). Upon re-expansion of the film at a lower surface pressure, the buckled structures are rapidly reincorporated into the film to re-form a flat monolayer (*18*, *19*). SP-B is a critical component in the formation of SP-A−DPPC tubular myelin structures that are thought to be important in the transport of lipid from the aqueous subphase to the lipid monolayer (*20*, *21*). These observations suggest that SP-B plays a critical role in maintaining the molecular continuity of the monolayer of the lipid and peptide at the air−water interface during breathing, as well as facilitating the incorporation of lipid from the lung aqueous subphase into the lipid monolayer at the alveolar air−water interface.

SP-B (*22*) is a small ($MW_{monomer} \sim 8.7$ kDa), lipid-associating protein that belongs to the saposin protein superfamily (*23*, *24*). SP-B is found in the mammalian lung as a covalently linked homodimer. Transgenic mice expressing only monomeric SP-B have normal longevity but significantly inhibited lung hysteresis, and surfactant from these mice was less able to reduce surface tension on a Wilhelmy balance (*23*). Like other members of the saposin superfamily, SP-B has a dominant amphipathic helical conformation in lipids and in structure-promoting solvents (*25*, *26*). Six conserved cysteines form three intrapeptide disulfide bonds and define a fold that has been conserved for an estimated 300 million years (*27*). The experimentally derived structures of three members of the superfamily, including saposin B [PDB entry 1N69 (*28*)], saposin C [PDB entry 1M12 (*29*)], and NK-lysin [PDB entry 1NKL (*30*)], all display this fold, although the helical splay of each of the proteins may differ.

One of the most interesting features of SP-B is the localization of cationic residues in the amphipathic helix regions of the N- and C-terminal segments of the protein. These positively charged segments likely provide important surfaces for interaction of the protein with lung surfactant phospholipids, especially phospholipids with anionic headgroups (*2*). The functional importance of anionic lipids is underlined by the observation that an anionic phospholipid, such as phosphatidylglycerol (PG), is a critical component of artificial lung surfactant (*31*).

Many of the *in vivo* and *in vitro* activities of SP-B can be mimicked to some extent by peptides containing subsegments of the full-length protein. Surfactant preparations containing synthetic peptides representing either N- or C-terminal segments of SP-B improve oxygenation and lung compliance in surfactant-deficient animal models (*32*, *33*). A peptide comprised of the 25 N-terminal residues of SP-B (*16*) facilitates dynamic respreading (*34*) and improves lung function in premature and lavaged rats (*35*). Another peptide design strategy has used the Leu-Leu repeat sequence in the C-terminal helical region of SP-B (residues 57−63) as a molecular template for the synthetic peptide KL_4 (Surfaxin) (*36*). This peptide does not have the *in vitro* and *in vivo* efficacy observed for native and synthetic SP-B sequences (*37*) but has shown some promise as a bronchoalveolar lavage for improving lung function in meconium aspiration syndrome (*38*).

High-resolution structural data for SP-B and SP-B-based peptides are critical in understanding the molecular mechanisms by which SP-B functions, as well as improving therapeutic interventions for RDS and ARDS. Residue specific structural information about the N-terminal and adjacent midsequence of SP-B has been determined in surfactant lipid using isotope-enhanced FTIR [PDB entry 1DFW (*39*)] and in the structure-promoting solvent methanol using solution NMR [PDB entry 1KMR (*40*)]. In this study, we use solution NMR to examine the structure of the C-terminal segment of human SP-B in two environments, the fluorinated alcohol hexafluoro-2-propanol (HFIP), which is known to be effective in inducing secondary structure in peptides, and in micelles composed of the anionic detergent sodium dodecyl sulfate (SDS).

MATERIALS AND METHODS

Peptide Synthesis and Purification. $SP\text{-}B_{63-78}$ (NH_2-GRMLPQLVCRLVLRCS-COOH) with amide ^{15}N labels at leucines 4, 7, 11, and 13 and valines 8 and 10 was synthesized by solid phase peptide synthesis employing *O*-fluorenylmethyl-oxycarbonyl (Fmoc) chemistry. Fmoc amino acids were supplied by AnaSpec, as were coupling agents. ^{15}N-labeled amino acids were obtained from Cambridge Isotope Laboratories and converted to their Fmoc derivatives by AnaSpec. Organic solvents and other reagents used for peptide synthesis and purification were high-performance liquid chromatography (HPLC) grade or better (Fisher Scientific, Aldrich Chemical). The ^{15}N-labeled peptide was synthesized at a 0.25 mmol scale with an ABI 431A peptide synthesizer configured for FastMoc double-coupling cycles for all residues to optimize yield (*41*). The peptide was assembled on a prederivatized N-Fmoc-*O*-*tert*-butylserine HMP resin (AnaSpec). Deprotection and cleavage of the peptide from the resin were carried out using a TFA/thioanisole/EDT/phenol/water mixture (10:0.5:0.25:0.5:0.5 by volume) followed by cold precipitation with *tert*-butyl ether. The crude product was then purified by preparative reverse phase HPLC with a Vydac C-18 column, using a water/acetonitrile linear gradient with 0.1% trifluoroacetic acid as an ion pairing agent. The molecular weight of the peptide was confirmed by fast atom bombardment or MALDI-TOF mass spectrometry and its >95% purity determined by analytical HPLC. The peptide was lyophilized and stored at 4 °C.

NMR and Structure Calculations. NMR experiments were carried out under two sample conditions: organic solvent and detergent micelles. For the organic solvent sample, the peptide was dissolved in 40% hexafluoro-2-propanol (HFIP), 50% H_2O, 10% D_2O, and 2 mM DSS (pH 3) with a peptide concentration of 2 mM, and NMR spectra were obtained at 5 °C. A second peptide sample was dissolved in 90% H_2O, 10% D_2O, 200 mM deuterated sodium dodecyl sulfate (SDS) (from Cambridge Isotope Laboratories), and 2 mM DSS (pH 6.9) with a peptide concentration of 2 mM and NMR data collection at 25 °C.

Two-dimensional (2D) spectra were acquired on a Bruker Avance 500 MHz spectrometer and three-dimensional (3D)

data on a Bruker Avance 700 MHz spectrometer, both equipped with *z*-gradients and triple-resonance TXI probes. Initial studies used one-dimensional (1D) proton and 2D $^{15}N-^{1}H$ HSQC spectra to aid in the choice of sample conditions. Frequency assignments were based on 2D homonuclear NOESY (mixing time of 100−300 ms) with watergate water suppression (typically 64−128 scans) and TOCSY (mixing time of 80 ms) (typically 64 scans) and 3D ^{15}N-edited NOESY.

To determine the position of the peptide within the micelles, 0.6 and 1.2 mM 5-doxylstearic acid (DSA) was added to the sample, $^{15}N-^{1}H$ HSQC and 2D TOCSY spectra were acquired, and the reduction in peak intensity was measured. A small amount of nondeuterated SDS was added to the final sample, and an additional 2D NOESY experiment was performed in an effort to identify SDS−peptide NOEs. While the SDS resonances could be clearly seen (at 4.00, 1.66, 1.33, and 0.86 ppm), no NOEs to the peptide were observed.

Spectra were processed using NMRPipe (*42*), and analysis was aided by NMRView (*43*). For both conditions, frequency assignments were obtained for all nuclei expected to be observable. The N-terminal amino group was not assigned, and in most cases, it was not possible to make stereospecific assignments. NOEs were quantified using the peak volume from the 2D NOESY spectra using a mixing time of 250 ms for the peptide in HFIP and 150 ms for the peptide in SDS. For HFIP, 79 sequential, 48 medium-range, and 28 ambiguous NOEs were defined, and for SDS, 67 sequential, 60 medium-range, and 87 ambiguous NOEs were defined. Ambiguous NOEs were assigned in cases in which up to four different inter-residue assignment possibilities existed.

Structure calculations made use of hydrogen bond and dihedral angle restraints where secondary structure could be clearly determined from local NOE patterns (Figure 4). Using these criteria, residues 68−78 in HFIP and residues 69−78 in SDS were determined to be α-helical and assigned hydrogen bond restraints ($H_{i+4}\cdots O_i$ = 2.5 Å and $N_{i+4}\cdots O_i$ = 3.5 Å) and dihedral angle restraints ($\phi = -60 \pm 30°$, $\varphi = 120 \pm 40°$).

A special structure calculation strategy was designed to address the large number of ambiguous NOEs and to fully sample all conformational space consistent with experimental data. Initially, 500 structures were calculated using the simulated annealing algorithm within CNS 1.2 (*44*) with restraints derived from the unambiguous NOEs and a list of NOEs that randomly assigned one of the possible assignments for each ambiguous NOE. This produced a wide variety of structures that satisfied at least a large portion of the experimental data. This set of structures was analyzed using Ensemble (*45*), a software package that was developed to weight structures of conformationally heterogeneous peptides to indicate the relative prevalence of different conformations. Since SP-B_{CTERM} does not appear to be conformationally heterogeneous under the conditions that were chosen, Ensemble was employed instead in indicating which structures best fit the experimentally derived ambiguous and unambiguous NOEs. A small number of structures were highly weighted by Ensemble (for HFIP, five of 200 structures contributed more than 73% to the ensemble; for SDS, six of 200 structures contributed more than 67% to the ensemble), and these were subjected to further refinement with CNS, using the unambiguous NOEs as well as the ambiguous NOEs implemented using the CNS "OR" statement. For each of the two experimental conditions, a total of 40 refined structures were produced and the 10 lowest-energy structures were retained for analysis. This set of 10 structures included structures derived from at least four of the structures highly rated using Ensemble. The frequency assignments have been deposited in the BioMagResBank (entry 4060) and the structure coordinates in the Protein Data Bank (entries 1RG3 and 1RG4).

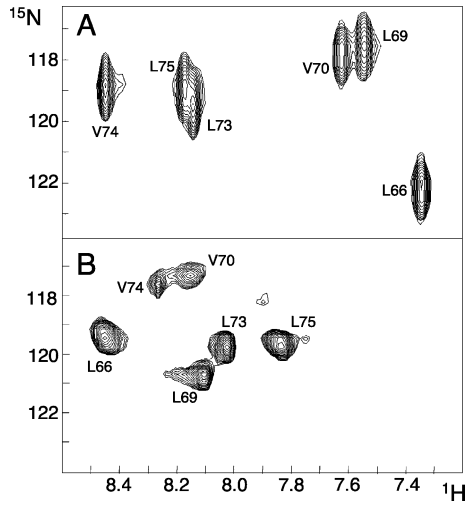

FIGURE 1: $^{15}N-^{1}H$ HSQC spectra of partially ^{15}N-labeled SP-B_{CTERM} [all L and V residues (six) labeled with ^{15}N] in 40% HFIP at 5 °C and pH 3 (A) and in 100:1 SDS at 25 °C and pH 6.9 (B). Resonance assignments are given.

RESULTS

The peptide used in these studies was composed of residues 63−78 of human SP-B (hereafter termed SP-B_{CTERM}) and was produced by chemical synthesis. Preliminary studies used circular dichroism (CD) to assess the secondary structure of the non-isotope-labeled peptide in various solvent conditions, including organic solvents, fluorinated alcohols, and detergents (data not shown). The data were deconvoluted using Selcon (*46*) to estimate the percentage of helix present under each condition. In a 2:3 (v:v) hexafluoro-2-propanol (HFIP)/water mixture, the CD indicated that ∼52% of SP-B_{CTERM} was helical. In a 70:1 (molar ratio) sodium dodecyl sulfate (SDS)/peptide mixture, the secondary structure content was similar (47% α-helix). Other solvents, such as trifluoroethanol (TFE), lead to lower α-helical and increased β-sheet content in SP-B_{CTERM}. In the solvent systems in which a greater β-sheet content was measured, we observed significant aggregation over time, possibly due to the formation of amyloid-like aggregates.

For the NMR work, the same peptide was synthesized with ^{15}N isotope labels on all valine (two) and leucine (four) residues. NMR structures for SP-B_{CTERM} were determined for the peptide in both 40% HFIP and SDS micelles (100:1 SDS:peptide ratio). The HFIP sample was analyzed by NMR $^{15}N-^{1}H$ HSQC and 1D proton NMR spectra between 5 and 45 °C. The HN resonances appeared to be least overlapped at 5 °C (Figure 1A), and therefore, this temperature was chosen for structural analysis. However, the spectra at higher temperatures were consistent with a degree of helical secondary structure similar to that present at the lower

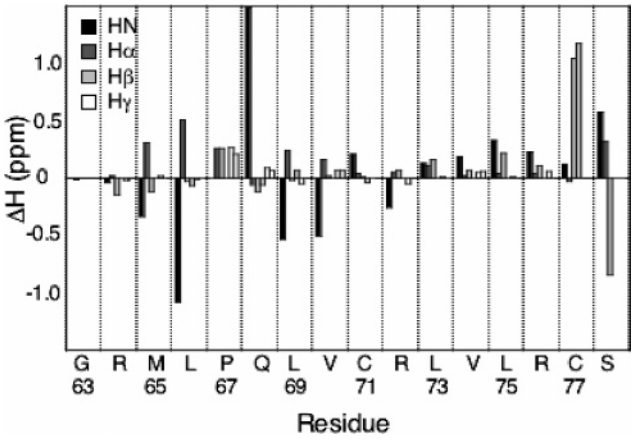

FIGURE 2: Differences in chemical shifts of SP-B_{CTERM} HN, Hα, Hβ, and Hγ resonances between HFIP and SDS. Values were calculated by subtracting the SDS chemical shifts from the HFIP chemical shifts.

temperature. Initial spectra of the peptide in SDS at 25 °C showed that all the ^{15}N-labeled residues were resolved and indicated only minor amounts of structural inhomogeneity, as evidenced by some very weak peaks in addition to the six expected ones (Figure 1B).

Resonance frequency assignments were determined for both conditions (see the Supporting Information) and are compared in Figure 2. Figure 3 shows a subsection of the 2D NOESY spectra with selected NOE assignments (which indicate spatial proximity) labeled. As expected, the cross-peak line widths for the SDS sample were significantly broader than in the HFIP sample. This lead to greater overlap and hence a larger portion of the NOEs that could not be unambiguously assigned. NOEs indicative of secondary structure as well as the Hα chemical shift index (CSI) are shown in Figure 4. Hα/β_i−HN_{i+3} NOEs indicated an α-helical conformation for at least residues 68−78 in HFIP and at least residues 69−78 in SDS. Hα CSI values suggest that in SDS, the helix extends from residue 67 to 78, but this could not be confirmed using NOEs due to overlap with intraresidue peaks. Significant positive CSI values and strong $H\alpha_i$−HN_{i+3} NOEs in the N-terminal region of the peptide in HFIP suggest this segment tends to take on an extended conformation in HFIP.

The structure of SP-B_{CTERM} in HFIP was calculated with 79 sequential, 48 medium-range and 28 ambiguous NOEs, and the SDS structures were calculated with 67 sequential, 60 medium-range, and 87 ambiguous NOEs. Ambiguous NOEs were used when two to four possible inter-residue assignments were evident for a cross-peak. To make the best possible use of the ambiguous NOEs, a special structure calculation strategy was employed.

Use of explicitly ambiguous NOEs (for example, by using the OR statement of CNS) in structure calculations generally results in poor sampling of the full set of conformational states consistent with all the possible assignments of an ambiguous NOE. To mitigate this difficulty, a structure calculation strategy was designed to more fully sample the conformational space consistent with the experimental data. An initial set of structures was calculated using the list of unambiguous NOEs and a list of NOEs that randomly assigned one of the possible assignments for each ambiguous NOE. This produced a wide variety of structures that satisfied at least a large portion of the experimental data. This set of structures was analyzed using Ensemble (*45*). Ensemble was initially developed to weight by probability structures of conformationally heterogeneous peptides and hence indicates the relative prevalence of different conformations. SP-B_{CTERM} does not appear to be conformationally heterogeneous under the conditions that were chosen. Therefore, Ensemble was employed instead in indicating which structures best fit the experimentally derived ambiguous and unambiguous NOEs. The structures most highly weighted by Ensemble were subjected to further refinement, using the unambiguous NOEs as well as the ambiguous NOEs (implemented using CNS OR statements). This structure calculation strategy was applied to both the SDS and HFIP data sets to produce ensembles of structures that fulfill the experimentally derived restraints (Figure 5).

The position of the peptide within the SDS micelles was probed using 5-doxylstearic acid (DSA), which is a molecule containing a paramagnetic moiety and an acyl chain that positions it among the acyl chains of the SDS micelles (*47*). Addition of DSA leads to broadening of peaks from nearby nuclei and thus a reduction in observed peak intensity, with the greatest intensity reductions occurring for the atoms that are closest to the DSA and hence the acyl chains of the SDS. The reduction in TOCSY HN−Hα and ^{15}N−^{1}H HSQC peak intensity was measured at 0.6 and 1.2 mM DSA (Figure 6). A few of the TOCSY HN−Hα resonances were very weak

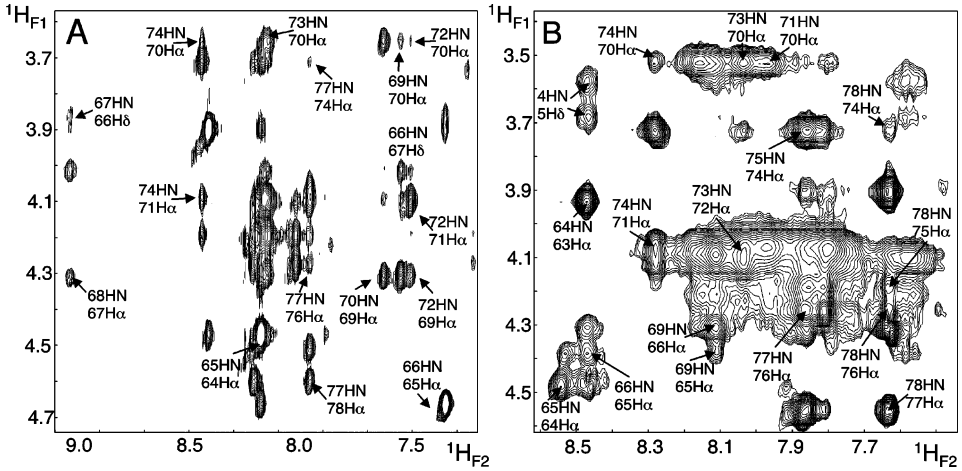

FIGURE 3: HN−Hα region of 2D NOESY spectra (mixing time of 150 ms) of SP-B_{CTERM} in (A) HFIP and (B) SDS. Selected inter-residue NOEs are labeled.

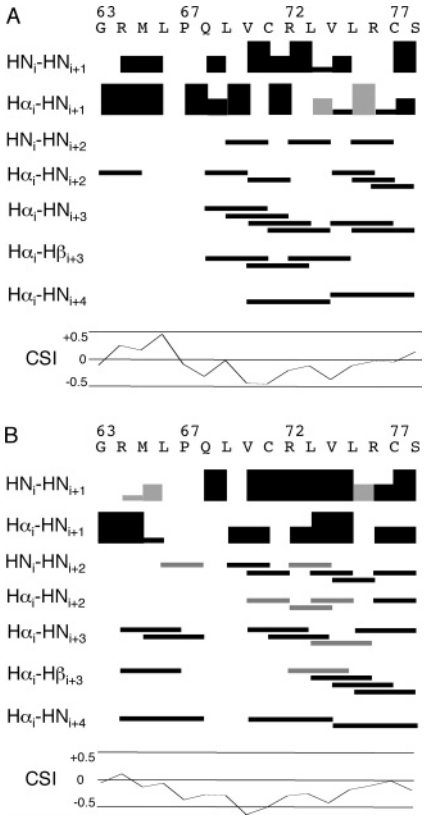

FIGURE 4: Secondary structure indicators for SP-B_{CTERM} in HFIP (A) and SDS (B). Black bars indicate unambiguous NOEs, and gray bars indicate ambiguous inter-residue (up to four-way) NOEs, i.e., peaks that were consistent with the indicated assignment but may also have been due to another inter-residue NOE. Strong, medium, and weak classifications are indicated by the height of the bar for the sequential NOEs. Note that many potential NOEs are marked as not observed because they could not be clearly identified in the spectra due to overlap with intraresidue peaks. The lower portion of each panel shows the chemical shift index (CSI) for the Hα resonances. CSI values close to zero are indicative of a random coil conformation, significantly negative values of a helical conformation, and significantly positive values of an extended (β-strand) conformation. The random coil values used in the CSI calculations were taken from ref *52* for the HFIP data (5 °C) and from ref *56* for the SDS data (25 °C).

even in the DSA-free sample due to the weak scalar coupling between HN and Hα protons in α-helices, and several more became too weak to measure after DSA addition; therefore, $^{15}N-^{1}H$ HSQC data were used to supplement the TOCSY data. Residues 66, 73, and 74 exhibited greater than average intensity reduction and are thus relatively close to DSA and the interior of the micelles. Residues 64, 65, 72, 77, and 78 exhibited less than average intensity reduction and are thus relatively far from the acyl chains of SDS; i.e., these residues face outward from the micelle. When mapped onto the structure, these define two opposite faces of the peptide (Figure 5B). Note that although only a relatively mild TOCSY peak intensity drop for residue 69 was observed, at 1.2 mM DSA its HSQC peak disappeared; therefore, this peak is marked as having no consensus result.

DISCUSSION

The sequence of SP-B is homologous to those of proteins such as NK-lysin (*30*), saposin B (*28*), and saposin C (*29*), for which three-dimensional structures have been determined. Thus, the SP-B monomer can be expected to consist of a

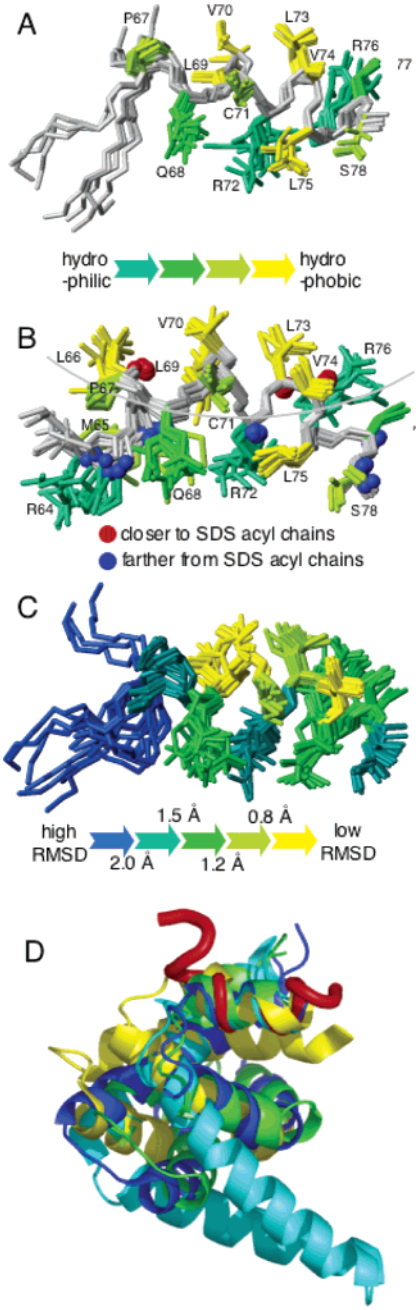

FIGURE 5: Structure of SP-B_{CTERM}. (A) Ensemble of 10 structures of the peptide in HFIP. The backbone is gray, and side chains (heavy atoms only) are colored. The side chains are colored according to their hydrophobicity (see key). For clarity, disordered side chains of residues 1−4 are not shown. (B) Ensemble of 10 structures of the peptide in SDS micelles. The coloring is as in panel A. Red spheres represent atoms with peaks that showed reduction more severe than average 5-DSA-induced peak intensity reduction and hence are positioned closer to the acyl chains of SDS. Blue spheres represent atoms that exhibited reduction less severe than average DSA-induced peak intensity reduction and hence are positioned away from the SDS acyl chains. The gray arc represents the surface of a 50 Å diameter SDS micelle; note that this is shown merely to indicate the degree of curvature of the micelle surface, not to indicate a particular depth of the peptide. (C) Alignment of SP-B_{CTERM} HFIP and SDS structure ensembles colored by heavy atom rmsd from the mean structure (see key). (D) Overlay of the SP-B_{CTERM} SDS structure (red) and saposin B (cyan) [PDB entry 1N69 (*28*)], saposin C (blue) [PDB entry 1M12 (*29*)], NK-lysin (green) [PDB entry 1NKL (*30*)], and granulysin (yellow) [PDB entry 1LN9 (*57*)]. Panels A−C were prepared using MolMol (*58*), and panel D was prepared with PyMOL (*59*).

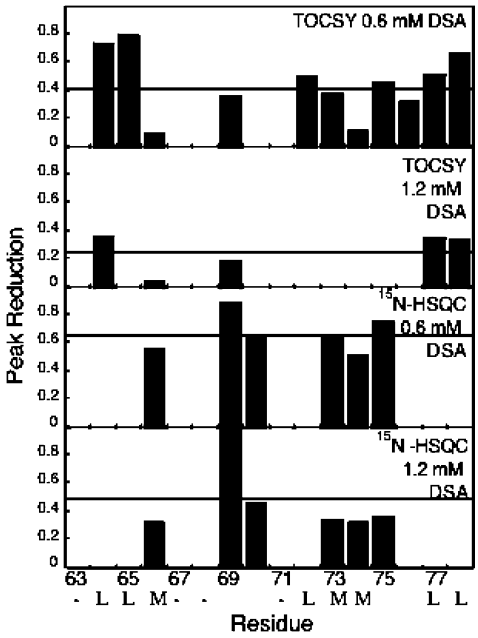

FIGURE 6: Reduction in TOCSY HN−Hα and $^{1}H-^{15}N$ HSQC peak intensity with the addition of 0.6 and 1.2 mM DSA. Values were computed as the fractional reduction in peak intensity from the DSA-free sample. Grey horizontal lines show the average fractional reduction for each plot. Below the residue number is the consensus result: L for reduction less severe than average DSA-induced reduction (i.e., fractional peak reduction closer to 0), M for reduction more severe than average DSA-induced reduction (i.e., fractional reduction closer to 1), blank for residues for which no definite trend could be discerned, and −for residues for which it was not possible to obtain a measurement (due to weak or overlapped peaks).

bundle of four or five helices, stabilized by three disulfide bonds, two of which link the C-terminal and N-terminal helices. The structure of segments of SP-B from near its N-terminus has previously been probed in lipid by FTIR (*39*) and in methanol by NMR (*40*). This study examines the structure of the 16 C-terminal residues of SP-B ($SP\text{-}B_{CTERM}$) which contains the predicted C-terminal helix and several residues N-terminal to the putative helix. A similar C-terminal peptide has been shown to possess partial biological activity (*32*). Since determination of the structure of full-length SP-B has long been hampered by its high degree of hydrophobicity, structural studies of the C-terminal peptide were initiated to add to our understanding of SP-B's mechanism of function.

NMR structures of the peptide were determined both in the fluorinated alcohol, HFIP, and in detergent micelles. SDS was deemed to be an appropriate choice of micelle detergent because it has a negatively charged headgroup. Electrostatic interactions between SP-B and anionic lipids have been shown to be important in the functional interactions of SP-B with bilayers and monolayers (*48*). Such interactions are likely to be important in promoting contact between the surfactant monolayer on the alveolar surface and bilayer structures in the subphase surfactant reservoir. Although SDS micelles can be expected to better mimic the *in vivo* bilayer environment than HFIP, we opted to use HFIP as well for two reasons: (1) to help in the analysis of the SDS spectra (which have much broader lines than the HFIP spectra) and (2) to give clues about the structural consequences of interactions between the positively charged residues on the peptide with the headgroups of anionic lipids. In both environments, the 10 or 11 C-terminal residues of $SP\text{-}B_{CTERM}$ take on a well-defined α-helical structure (Figure 5). In HFIP, the N-terminal segment of the peptide appears to be in a poorly defined, extended structure, whereas in SDS, these residues take on a well-defined, semicompact structure.

The fluorinated alcohol, TFE, is commonly used in NMR studies to induce secondary structure in proteins and peptides that would otherwise be unstructured. HFIP appears to have an even stronger secondary structure-inducing effect than TFE but, to date, has been much less commonly used in NMR studies. Currently, no widespread consensus about the mechanism by which these solvent systems induce secondary structure has been reached, although strengthening of both intrapeptide hydrogen bonds and intrapeptide local hydrophobic interactions is likely to be important in TFE or HFIP stabilization of secondary structure (*49*−*51*).

Many structure determinations of membrane-associated peptides are performed in organic solvent rather than in micelles. Hence, it is of general interest to analyze which structural features are the same or different between structures determined in HFIP and SDS. This comparison also provides clues about the role of anionic lipid headgroups in defining the structure of SP-B. HFIP provides a convenient reference structure, as in preliminary studies, $SP\text{-}B_{CTERM}$ did not produce informative NMR spectra in zwitterionic detergent micelles such as DPC. The structures determined in HFIP and SDS are very similar in the α-helical region (residues 66−78) and most disparate in the N-terminal region, which is poorly defined and extended in HFIP but well-defined and compact in SDS (Figure 5C). Both structures show an amphipathic distribution of hydrophobic and hydrophilic side chains (Figure 5A,B), although the SDS structure displays a slightly better defined partitioning between hydrophobic and hydrophilic side chains. The position of the helix side chains was more similar between the two solvents on the hydrophobic face than on the hydrophilic face (Figure 5C) which indicates that HFIP does a better job of mimicking the hydrophobic elements of the more membrane-mimetic SDS micelles than it does of mimicking the hydrophilic elements. It should be noted that the while the SDS and HFIP experiments were performed at different pHs (6.9 and 3), this is expected to have very little, if any, effect on structure, since the only chemical group on the peptide that may change in charge between these two pHs is the C-terminal carboxyl group.

The positioning of the peptide within the SDS micelles was probed using the paramagnetic molecule DSA (Figure 5B). For the helical portion of the peptide, these experiments indicated one face was oriented toward the interior of the micelle and one face pointed toward the exterior. The interior and exterior faces defined by the DSA experiments corresponded well with the hydrophobicity of the side chains. The residues that appeared to be located farthest from the micelle interior were those at the N-terminus of the peptide. Altogether, the DSA results indicate that the peptide is positioned at the water interface with the hydrophobic face of the helix close to the acyl chains of SDS, the hydrophilic face of the helix toward the SDS polar headgroup−water interface, and the irregularly shaped N-terminus extending even farther from the micelle than the hydrophilic helix face.

Chemical shifts (resonance frequencies) are very sensitive probes for changes in protein conformation, and so it is

interesting to compare the chemical shifts for the peptide in HFIP and SDS. For residues 68−76, the Hα, Hβ, and Hγ resonances change very little between HFIP and SDS (Figure 2), indicating these residues take on a similar structure in the two solvent systems. Conversely, the five N-terminal and two C-terminal residues exhibit a greater difference in conformation between the two solvent systems. The HN chemical shift is known to be especially sensitive to changes in the solvent system because it reflects changes in bonding of hydrogen to the solvent (*52*, *53*). The largest HN chemical shift changes occurred in the N-terminal, non-α-helical, segment of SP-B_{CTERM} which is consistent with observations that solvent-exposed amide protons are more affected by a change in solvent composition than intrapeptide hydrogen-bonded protons (*54*). It is interesting to note that residues 66 and 68, which are located on opposite faces of the peptide, had the largest HN chemical shift changes of all the residues, but the changes were of opposite sign.

Modification in peptide conformation with the change in environmental conditions has also been observed for N-terminal peptides of SP-B. Although residues 9−36 of SP-B have a relatively stable conformation, the adjacent segment has been shown to have some reversible conformational polymorphism that is dependent on the surface pressure of the surfactant lipid monolayer (*55*). Such fine-tuning of SP-B's conformation in response to pressure and the presence of anionic lipids may underlie SP-B's critical functional role in lung surfactant.

These studies indicate that the C-terminal segment of SP-B has a stable amphipathic helix similar to the structural motifs of the other saposin structures (Figure 5D) and to a theoretical model of SP-B templated on the backbone structure of NK-lysin (*24*). The differences in the structures observed in HFIP and SDS highlight the structural and resultant functional consequences of interactions between SP-B and lipid molecules, especially between positively charged peptide side chains and negatively charged lipid headgroups. Subtle differences in the structure between HFIP and SDS were seen in the conformation of the side chains in the helical region of the peptide, especially on the hydrophilic face. However, the most significant differences were found in the N-terminal nonhelical region. This N-terminal region of the peptide corresponds to the loop between the last and second-to-last helices of the full-length protein, and thus, the conformation of this region might have a significant impact on the overall topology of the protein, by helping to define the relative orientations of the helices. The relative position of the helices in the saposin superfamily proteins appears to be quite variable with NK-lysin (*30*) and saposin C (*29*) taking on a fairly compact structure, but saposin B (*28*) taking on a fairly open structure (Figure 5D). It is still unclear how open or closed the tertiary structure of full-length SP-B might be. If the *in vivo* tertiary structure of SP-B is fairly open, the structure of the interhelical loops may be quite important in defining the tertiary structure of the protein.

ACKNOWLEDGMENT

We thank Brian Dawson and Health Canada for acquiring part of the NMR data used in this study on the Health Canada 700 MHz spectrometer.

SUPPORTING INFORMATION AVAILABLE

^{1}H and ^{15}N chemical shift assignments for SP-B_{CTERM}. This material is available free of charge via the Internet at http://pubs.acs.org.

REFERENCES

1. Goerke, J. (1998) Pulmonary surfactant: functions and molecular composition, *Biochim. Biophys. Acta 1408*, 79−89.
2. Perez-Gil, J. (2002) Molecular interactions in pulmonary surfactant films, *Biol. Neonate 81* (Suppl. 1), 6−15.
3. McCormack, F. X. (1998) Structure, processing and properties of surfactant protein A, *Biochim. Biophys. Acta 1408*, 109−131.
4. Crouch, E. C. (1998) Structure, biologic properties, and expression of surfactant protein D (SP-D), *Biochim. Biophys. Acta 1408*, 278−289.
5. Hawgood, E. A. (1998) Structure and properties of surfactant protein B, *Biochim. Biophys. Acta*.
6. Avery, M. E., and Mead, J. (1959) Surface properties in relation to atelectasis and Hyaline membrane disease, *AMA J. Dis. Child. 97*, 517−523.
7. Hartog, A., Gommers, D., and Lachmann, B. (1995) Role of surfactant in the pathophysiology of the acute respiratory distress syndrome (ARDS), *Monaldi Arch. Chest. Dis. 50*, 372−377.
8. Schwartz, R. M., Luby, A. M., Scanlon, J. W., and Kellogg, R. J. (1994) Effect of surfactant on morbidity, mortality, and resource use in newborn infants weighing 500 to 1500 g, *N. Engl. J. Med. 330*, 1476−1480.
9. Rodriguez, R. J., and Martin, R. J. (1999) Exogenous surfactant therapy in newborns, *Respir. Care Clin. N. Am. 5*, 595−616.
10. Lewis, J. F., and Veldhuizen, R. (2003) The role of exogenous surfactant in the treatment of acute lung injury, *Annu. Rev. Physiol. 65*, 613−642.
11. Nogee, L. M., Garnier, G., Dietz, H. C., Singer, L., Murphy, A. M., deMello, D. E., and Colten, H. R. (1994) A mutation in the surfactant protein B gene responsible for fatal neonatal respiratory disease in multiple kindreds, *J. Clin. Invest. 93*, 1860−1863.
12. Clark, J. C., Wert, S. E., Bachurski, C. J., Stahlman, M. T., Stripp, B. R., Weaver, T. E., and Whitsett, J. A. (1995) Targeted disruption of the surfactant protein B gene disrupts surfactant homeostasis, causing respiratory failure in newborn mice, *Proc. Natl. Acad. Sci. U.S.A. 92*, 7794−7798.
13. Robertson, B., Kobayashi, T., Ganzuka, M., Grossmann, G., Li, W. Z., and Suzuki, Y. (1991) Experimental neonatal respiratory failure induced by a monoclonal antibody to the hydrophobic surfactant-associated protein SP-B, *Pediatr. Res. 30*, 239−243.
14. Glasser, S. W., Burhans, M. S., Korfhagen, T. R., Na, C. L., Sly, P. D., Ross, G. F., Ikegami, M., and Whitsett, J. A. (2001) Altered stability of pulmonary surfactant in SP-C-deficient mice, *Proc. Natl. Acad. Sci. U.S.A. 98*, 6366−6371.
15. Nogee, L. M., Dunbar, A. E., III, Wert, S. E., Askin, F., Hamvas, A., and Whitsett, J. A. (2001) A mutation in the surfactant protein C gene associated with familial interstitial lung disease, *N. Engl. J. Med. 344*, 573−579.
16. Longo, M. L., Bisagno, A. M., Zasadzinski, J. A., Bruni, R., and Waring, A. J. (1993) A function of lung surfactant protein SP-B, *Science 261*, 453−456.
17. Lipp, M. M., Lee, K. Y., Zasadzinski, J. A., and Waring, A. J. (1996) Phase and morphology changes in lipid monolayers induced by SP-B protein and its amino-terminal peptide, *Science 273*, 1196−1199.
18. Lipp, M. M., Lee, K. Y. C., Takmoto, D. Y., Zasadzinski, J. A., and Waring, A. J. (1998) Co-existence of buckled and flat monlayers, *Phys. Rev. Lett. 81*, 1650−1653.
19. Ding, J., Doudevski, I., Warriner, H. E., Alig, T., Zasadzinski, J. A., Waring, A. J., and Sherman, M. A. (2003) Nanostructure changes in lung surfactant monolayers induced by interactions between POPG and surfactant protein B (SP-B), *Langmuir 19*, 1539−1550.
20. Suzuki, Y., Fujita, Y., and Kogishi, K. (1989) Reconstitution of tubular myelin from synthetic lipids and proteins associated with pig pulmonary surfactant, *Am. Rev. Respir. Dis. 140*, 75−81.
21. Williams, M. C., Hawgood, S., and Hamilton, R. L. (1991) Changes in lipid structure produced by surfactant proteins SP-A, SP-B, and SP-C, *Am. J. Respir. Cell Mol. Biol. 5*, 41−50.
22. Xu, J. J., Richardson, C., Ford, C., Spencer, T., Yao, L. J., Mackie, G., Hammond, G., and Possmayer, F. (1989) Isolation and

characterization of the cDNA for pulmonary surfactant-associated protein-B (SP-B) in the rabbit, *Biochem. Biophys. Res. Commun. 160*, 325−332.
23. Beck, D. C., Na, C. L., Whitsett, J. A., and Weaver, T. E. (2000) Ablation of a critical surfactant protein B intramolecular disulfide bond in transgenic mice, *J. Biol. Chem. 275*, 3371−3376.
24. Zaltash, S., Palmblad, M., Curstedt, T., Johansson, J., and Persson, B. (2000) Pulmonary surfactant protein B: a structural model and a functional analogue, *Biochim. Biophys. Acta 1466*, 179−186.
25. Vandenbussche, G., Clercx, A., Clercx, M., Curstedt, T., Johansson, J., Jornvall, H., and Ruysschaert, J. M. (1992) Secondary structure and orientation of the surfactant protein SP-B in a lipid environment. A Fourier transform infrared spectroscopy study, *Biochemistry 31*, 9169−9176.
26. Cruz, A., Casals, C., and Perez-Gil, J. (1995) Conformational flexibility of pulmonary surfactant proteins SP-B and SP-C, studied in aqueous organic solvents, *Biochim. Biophys. Acta 1255*, 68−76.
27. Power, J. H., Doyle, I. R., Davidson, K., and Nicholas, T. E. (1999) Ultrastructural and protein analysis of the surfactant in the Australian lungfish *Neoceratodus forsteri* evidence for conservation of composition for 300 million years, *J. Exp. Biol. 202*, 2543−2550.
28. Ahn, V. E., Faull, K. F., Whitelegge, J. P., Fluharty, A. L., and Prive, G. G. (2003) Crystal structure of saposin B reveals a dimeric shell for lipid binding, *Proc. Natl. Acad. Sci. U.S.A. 100*, 38−43.
29. de Alba, E., Weiler, S., and Tjandra, N. (2003) Solution structure of human saposin C: pH-dependent interaction with phospholipid vesicles, *Biochemistry 42*, 14729−14740.
30. Liepinsh, E., Andersson, M., Ruysschaert, J. M., and Otting, G. (1997) Saposin fold revealed by the NMR structure of NK-lysin, *Nat. Struct. Biol. 4*, 793−795.
31. Weaver, T. E., and Conkright, J. J. (2001) Function of surfactant proteins B and C, *Annu. Rev. Physiol. 63*, 555−578.
32. Revak, S. D., Merritt, T. A., Hallman, M., Heldt, G., La Polla, R. J., Hoey, K., Houghten, R. A., and Cochrane, C. G. (1991) The use of synthetic peptides in the formation of biophysically and biologically active pulmonary surfactants, *Pediatr. Res. 29*, 460−465.
33. Walther, F. J., Hernandez-Juviel, J. M., Gordon, L. M., Sherman, M. A., and Waring, A. J. (2002) Dimeric surfactant protein B Peptide sp-b(1−25) in neonatal and acute respiratory distress syndrome, *Exp. Lung Res. 28*, 623−640.
34. Veldhuizen, E. J., Waring, A. J., Walther, F. J., Batenburg, J. J., van Golde, L. M., and Haagsman, H. P. (2000) Dimeric N-terminal segment of human surfactant protein B (dSP-B(1−25)) has enhanced surface properties compared to monomeric SP-B(1−25), *Biophys. J. 79*, 377−384.
35. Tanaka, Y., Takei, T., Aiba, T., Masuda, K., Kiuchi, A., and Fujiwara, T. (1986) Development of synthetic lung surfactants, *J. Lipid Res. 27*, 475−485.
36. Cochrane, C. G., and Revak, S. D. (1991) Pulmonary surfactant protein B (SP-B): structure−function relationships, *Science 254*, 566−568.
37. Walther, F. J., Hernandez-Juviel, J., Bruni, R., and Waring, A. J. (1998) Protein composition of synthetic surfactant affects gas exchange in surfactant-deficient rats, *Pediatr. Res. 43*, 666−673.
38. Wiswell, T. E., Knight, G. R., Finer, N. N., Donn, S. M., Desai, H., Walsh, W. F., Sekar, K. C., Bernstein, G., Keszler, M., Visser, V. E., Merritt, T. A., Mannino, F. L., Mastrioianni, L., Marcy, B., Revak, S. D., Tsai, H., and Cochrane, C. G. (2002) A multicenter, randomized, controlled trial comparing Surfaxin (Lucinactant) lavage with standard care for treatment of meconium aspiration syndrome, *Pediatrics 109*, 1081−1087.
39. Gordon, L. M., Lee, K. Y., Lipp, M. M., Zasadzinski, J. A., Walther, F. J., Sherman, M. A., and Waring, A. J. (2000) Conformational mapping of the N-terminal segment of surfactant protein B in lipid using ^{13}C-enhanced Fourier transform infrared spectroscopy, *J. Pept. Res. 55*, 330−347.
40. Kurutz, J. W., and Lee, K. Y. (2002) NMR structure of lung surfactant peptide SP-B(11−25), *Biochemistry 41*, 9627−9636.
41. Fields, C. G., Lloyd, D. H., Macdonald, R. L., Ottenson, K. M., and Nobel, R. L. (1991) HBTU activation for automated Fmoc solid-phase peptide synthesis, *Pept. Res. 4*, 95−101.
42. Delaglio, F., Grzesiek, S., Vuister, G. W., Zhu, G., Pfeifer, J., and Bax, A. (1995) NMRPipe: a multidimensional spectral processing system based on UNIX pipes, *J. Biomol. NMR 6*, 277−293.
43. Johnson, B., and Blevins, R. (1994) NMRView: A computer program for the visualization and analysis of NMR data, *J. Biomol. NMR 4*, 603−614.
44. Brunger, A. T., Adams, P. D., Clore, G. M., DeLano, W. L., Gros, P., Grosse-Kunstleve, R. W., Jiang, J. S., Kuszewski, J., Nilges, M., Pannu, N. S., Read, R. J., Rice, L. M., Simonson, T., and Warren, G. L. (1998) Crystallography & NMR system: A new software suite for macromolecular structure determination, *Acta Crystallogr. D54* (Part 5), 905−921.
45. Choy, W. Y., and Forman-Kay, J. D. (2001) Calculation of ensembles of structures representing the unfolded state of an SH3 domain, *J. Mol. Biol. 308*, 1011−1032.
46. Sreerama, N., Venyaminov, S. Y., and Woody, R. W. (1999) Estimation of the number of α-helical and β-strand segments in proteins using circular dichroism spectroscopy, *Protein Sci. 8*, 370−380.
47. Mascioni, A., Porcelli, F., Ilangovan, U., Ramamoorthy, A., and Veglia, G. (2003) Conformational preferences of the amylin nucleation site in SDS micelles: An NMR study, *Biopolymers 69*, 29−41.
48. Perez-Gil, J., Casals, C., and Marsh, D. (1995) Interactions of hydrophobic lung surfactant proteins SP-B and SP-C with dipalmitoylphosphatidylcholine and dipalmitoylphosphatidylglycerol bilayers studied by electron spin resonance spectroscopy, *Biochemistry 34*, 3964−3971.
49. Chiti, F., Taddei, N., Webster, P., Hamada, D., Fiaschi, T., Ramponi, G., and Dobson, C. M. (1999) Acceleration of the folding of acylphosphatase by stabilization of local secondary structure, *Nat. Struct. Biol. 6*, 380−387.
50. Luo, P., and Baldwin, R. L. (1997) Mechanism of helix induction by trifluoroethanol: a framework for extrapolating the helix-forming properties of peptides from trifluoroethanol/water mixtures back to water, *Biochemistry 36*, 8413−8421.
51. Gast, K., Zirwer, D., Muller-Frohne, M., and Damaschun, G. (1999) Trifluoroethanol-induced conformational transitions of proteins: insights gained from the differences between α-lactalbumin and ribonuclease A, *Protein Sci. 8*, 625−634.
52. Merutka, G., Dyson, H. J., and Wright, P. E. (1995) "Random coil" ^{1}H chemical shifts obtained as a function of temperature and trifluoroethanol concentration for the peptide series GGXGG, *J. Biomol. NMR 5*, 14−24.
53. Pitner, T. P., and Urry, D. W. (1972) Proton magnetic resonance studies in trifluoroethanol. Solvent mixtures as a means of delineating peptide protons, *J. Am. Chem. Soc. 94*, 1399−1400.
54. Urry, D. W., and Long, M. M. (1976) Conformations of the repeat peptides of elastin in solution: an application of proton and carbon-13 magnetic resonance to the determination of polypeptide secondary structure, *CRC Crit. Rev. Biochem. 4*, 1−45.
55. Flach, C. R., Cai, P., Dieudonne, D., Brauner, J. W., Keough, K. M., Stewart, J., and Mendelsohn, R. (2003) Location of Structural Transitions in an Isotopically Labeled Lung Surfactant SP-B Peptide by IRRAS, *Biophys. J. 85*, 340−349.
56. Wishart, D. S., and Nip, A. M. (1998) Protein chemical shift analysis: a practical guide, *Biochem. Cell Biol. 76*, 153−163.
57. Anderson, D. H., Sawaya, M. R., Cascio, D., Ernst, W., Modlin, R., Krensky, A., and Eisenberg, D. (2003) Granulysin crystal structure and a structure-derived lytic mechanism, *J. Mol. Biol. 325*, 355−365.
58. Koradi, R., Billeter, M., and Wuthrich, K. (1996) MOLMOL: A program for display and analysis of macromolecular structures, *J. Mol. Graphics 14*, 29−32.
59. DeLano, W. L. (2002) *The PyMOL User's Manual*, Delano Scientific, San Carlos, CA.

BI0481895